Numerical Simulation of Transpiration Cooling in a Laminar Hypersonic Boundary-Layer

Hassan Saad Ifti *, Tobias Hermann[†], and Matthew McGilvray[‡]
University of Oxford, Oxford, OX2 0ES, United Kingdom

James Merrifield[§]
Fluid Gravity Engineering Ltd., Emsworth, PO10 7DX, United Kingdom

Two-dimensional simulations of transpiration cooling in a laminar, hypersonic boundary-layer were performed using the Thermochemical Implicit Non-Equilibrium Algorithm (TINA) – a Navier-Stokes solver. Coolant concentration and heat flux results are compared to data obtained from laminar transpiration cooling experiments conducted in the Oxford High Density Tunnel (HDT) employing a flat-plate geometry at Mach 7. TINA successfully predicts the mixing rate at the wall as a function of the stream-wise direction for all blowing ratios. The simulations are more successful in predicting the mixing downstream of the injector compared to the mixing on the injector, especially at low blowing ratios. A collapse of the thermal effectiveness values calculated from simulation data is achieved, which agrees with laminar correlations within an absolute value of ±10%. It is shown that, when the concentration effectiveness is close to 1 at the injector, the temperature gradient becomes negative at locations immediately downstream of the injector, resulting in a negative heat flux. The acceleration of the coolant in the stream-wise direction downstream promotes dissipation of energy, which results in a reduction in the temperature of the coolant and thereby induces a negative temperature gradient close to the injector.

I. Introduction

Hypersonic vehicles, such as rockets or spaceplanes, are subject to extreme heat fluxes as a result of aerodynamic heating [1]. A thermal protection system (TPS) is therefore required to protect the vehicle from overheating. Transpiration cooling is a promising technology that could enable a re-usable TPS for hypersonic vehicles. It is an active cooling method where a coolant gas is injected through a porous material into the boundary-layer. The cooling process comprises three different effects (see Fig. 1): (a) heat from the wall is convected out by the coolant fluid; (b) the coolant gas

---

[*] DPhil Candidate, Oxford Thermofluids Institute, Department of Engineering Science, University of Oxford, Southwell Building, Osney Mead. Email: saad.ifti@eng.ox.ac.uk

[†] Lecturer, Oxford Thermofluids Institute, Department of Engineering Science, University of Oxford, Southwell Building, Osney Mead.

[‡] Associate Professor, Oxford Thermofluids Institute, Department of Engineering Science, University of Oxford, Southwell Building, Osney Mead.

[§] Senior Researcher, Fluid Gravity Engineering Ltd., The Old Coach House.

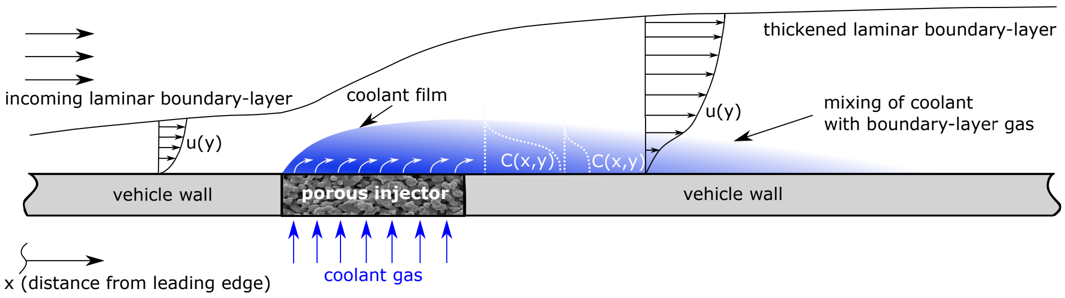

Fig. 1 Schematic of a flat surface with a porous, transpiration cooling injector (not to scale).

creates a film (blue) that insulates the wall underneath from the hot cross-flow; and (c) the coolant film protects the wall from free-stream Oxygen and thereby prevents oxidation of the wall, which enables the wall-material to operate at a higher temperature enhancing radiative cooling. The success of the latter two processes depends on the coolant film that is formed on and downstream of the injector. This protective film loses its concentration in the stream-wise direction and eventually diminishes at a downstream location as it mixes with the incoming hypersonic cross-flow (see the concentration gradient, $C(y)$ in Fig. 1).

There is a vast amount of work on the downstream mixing in turbulent boundary-layers [2, 3]. However, only a handful of studies [4–10] are concerned with the downstream mixing in a laminar boundary-layer. This is a limitation since hypersonic vehicles could face peak heating in the laminar regime [11]. The existing studies that compare numerical results to experiments are concerned with the heat flux reduction only. However, the coolant's concentration itself becomes an important quantity to understand the mixing process between the coolant gas and the boundary-layer gas since a direct relation between heat and mass transfer coefficient cannot be assumed in laminar flows unlike in turbulent cases. In particular, studies comparing numerical results to experimentally obtain coolant concentration are not available in the literature.

In this paper, numerical simulations of transpiration cooling in a laminar, hypersonic flow are performed. The coolant concentration and heat flux reduction results are compared to laminar transpiration cooling experiments conducted at Mach 7 in the Oxford High Density Tunnel (HDT), where Pressure-sensitive Paint (PSP) and thin-film gauges were respectively used to measure the wall concentration and heat flux reduction downstream of the injector on a flat-plate [12].

II. Methodology

A. Experiments

Transpiration cooling experiments in a laminar boundary-layer employing a flat-plate model (see Fig. 2) were conducted in the Oxford High Density Tunnel (HDT) at Mach 7 (see Ref. [12] for details). The flat-plate model was at an angle of attack of AoA = 0°. A porous injector (39.5 mm × 39.5 mm) made of sintered zirconium diboride

(ZrB_2) was situated 160 mm downstream of the leading edge. The boundary-layer static pressure, temperature and wall temperature were respectively p_e = 542.04 Pa, T_e = 43.53 K, and T_w = 293 K. The total pressure and total temperature were p_0 = 1.738 MPa and T_0 = 470.1 K, respectively. The boundary-layer edge velocity was u_e = 925.9 ms^{-1}. The blowing ratios (Cases 1 to 6) are given in Table 1. For reference, the blowing ratio is defined as

$$F = \frac{\rho_c u_c}{\rho_e u_e} \tag{1}$$

and the blowing parameter as

$$B_h = \frac{F}{St_0}, \tag{2}$$

where ρ denotes the density and St_0 is the Stanton number at the injector location without blowing.

Pressure sensitive-paint (PSP) with an area of interrogation of 140 mm×37 mm was applied immediately downstream of the injector to measure the relative concentration of the injected coolant gas at the wall. The PSP was excited by an LED of 390 nm (centre wavelength) and the emitted, higher wavelength radiation was captured by a camera fitted with a red filter (lower wavelength cut-off: 550 nm). This excitation is quenched by Oxygen in the air, and therefore the illumination can be calibrated by collecting illumination data for different flow static pressures (measured by surface mounted Kulite pressure transducers) without coolant injection. By applying the same calibration to cases with coolant (foreign gas) injection, a trace of the film can be identified as the quenching is influenced by the film. Injected coolant gas (Nitrogen or Helium) hinders the quenching by displacing air in the boundary-layer. Comparing a case with air injection and one with a foreign gas injection at the same blowing ratio, gives a measure of how much air is displaced by the foreign gas, i.e. to what extent the coolant is forming a film. The concentration film effectiveness is defined as

$$\eta_c = 1 - \frac{p_{O_2,\,\text{foreign gas}}}{p_{O_2,\,\text{air}}}, \tag{3}$$

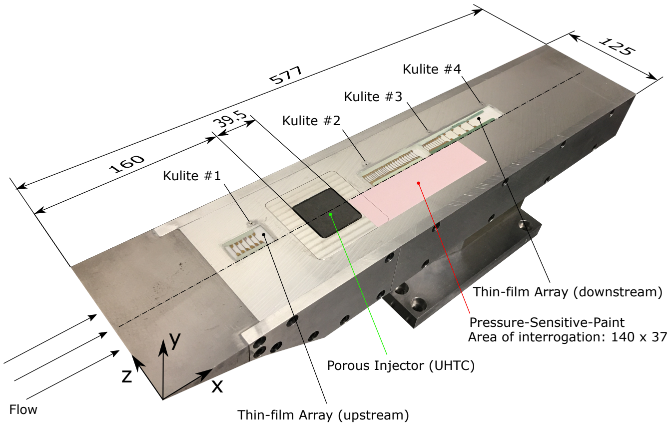

Fig. 2 Flat-plate model with PSP coat downstream of the porous injector. Reprinted with permission from Ifti et al. [12] (copyright 2022).

where $p_{O_2,\text{ air}}$ and $p_{O_2,\text{ foreign gas}}$ are Oxygen partial pressures with air and foreign gas injections, respectively, at the same blowing ratio. A span-wise average of 10 mm close to the centreline – where the film is two dimensional – is taken to reduce the data for η_c to one dimension, which varies only in the stream-wise direction, x.

Macor-based Platinum thin-film gauges installed upstream and downstream of the injector measured the heat fluxes, which were compared to Eckert's correlation [13] for laminar boundary-layers to ensure that the boundary-layer was laminar during the experiments. The heat flux reduction by transpiration cooling is formulated as the isothermal cooling effectiveness [6]

$$\eta_{th} = 1 - \frac{St_c}{St_0}, \tag{4}$$

where St is the Stanton number and the subscripts 'c' and '0' respectively denote cooled and uncooled cases. A case of 100% cooling, i.e. zero heat flux to the wall, would result in an effectiveness of 1. Eq.(4) is only valid for small blowing ratios and cases where the coolant gas is similar to the free-stream gas [5]. It is also invalid for locations that are in close proximity to the injector. The obtained values of η_{th} can be correlated by a factor defined by Heufer & Olivier [5] as

$$\xi = \frac{1}{Fs}\sqrt{\frac{x - x_s}{x_s^{1.16}}\frac{C^* x}{Re_u}}, \tag{5}$$

where x_s is the slot location from the leading edge, s is the slot length, and $C^* = (\rho^*\mu^*)^{0.5}(\rho_e\mu_e)^{-0.5}$ is the Chapman-Rubesin factor evaluated at Eckert's reference temperature [13]. Re_u is the unit Reynolds number and μ the viscosity. The effect of different coolant gases can be taken into account by multiplying the correlation factor, ξ, by the ratio of the specific heat capacities of the free-stream gas and the coolant gas, $c_{p,e}/c_{p,c}$, with an appropriate exponent, which has been demonstrated by Keller et al. [7]. Hombsch & Olivier [6] proposed a correlation obtained from experimental data expressed as

$$\eta_{th} = \begin{cases} 1 & \text{for } \xi \leq 0.96, \\ [1 + 0.38(\xi - 0.96)]^{-1.6} & \text{for } \xi > 0.96. \end{cases} \tag{6}$$

A modified correlation based on a new set of experimental data was proposed by Ifti et al. [12] given as

$$\eta_{th} = \begin{cases} 1 & \text{for } \xi \leq 0.96, \\ [1 + 0.4(\xi - 0.96)]^{-1} & \text{for } \xi > 0.96. \end{cases} \tag{7}$$

B. Numerical Approach

Two-dimensional simulations were performed employing the Thermochemical Implicit Non-Equilibrium Algorithm (TINA) – a Navier-Stokes solver developed by Fluid Gravity Engineering Ltd. for supersonic and hypersonic flows. TINA

Table 1 Overview of blowing cases.

Case	1	2	3	4	5	6
F [%]	0.0406	0.0818	0.153	0.295	0.0416	0.08
B_h [−]	1.49	2.99	5.59	10.8	1.52	2.93
Coolant gas	N_2	N_2	N_2	N_2	He	He

is a point or line implicit time marching solver with spatial gradient calculated to second-order accuracy. It employs an approximate Riemann solver in conjunction with flux limiters for the inviscid fluxes. A Total Variation-Diminishing (TVD) shock capturing algorithm is used which ensures non-oscillatory behaviour near shock waves at essentially any free stream Mach number. Air was used as the main flow, which – along with the coolant gas – was simulated as a perfect gas matching the flow conditions (non-reacting) in the experiments stated in Section II.A. Futher details can be found in Refs. [14, 15].

A flow over the flat-plate geometry described above was simulated. A computational domain of 340 mm × 58 mm was employed with a total of 50511 grid points. The grid is equidistant in the stream-wise direction ($\Delta x = 1 \times 10^3$ m) and stretched in the wall-normal direction with a first cell height of $\Delta y = 2.5 \times 10^{-6}$ m (elected based on a grid convergence study). This yielded a wall cell Reynolds number of $Re_{\text{cell}} < 1$, which ensures that the high gradients close to the wall are sufficiently resolved.

At the wall, the nodes between 160 mm and 200 mm were set to a permeable boundary condition, which prescribes the mass flux of the injected coolant gas. Simulations were run for all cases presented in Table 1.

The wall condition was set as isothermal at $T_w = 293$ K. The variation of species viscosity with temperature for Oxygen, Nitrogen, and Helium was modelled using Blottner curve fits [16]. Species thermal conductivity is derived from species viscosity using the Euken formula [17]. The mixture viscosity and thermal conductivity are calculated using Wilkie's mixing rule [18]. The diffusion velocity of each species is assumed to be proportional to the gradient in the species mole fraction only with species diffusion coefficient taken from the work of Lee [19]. Here, a baseline diffusion coefficient, D, is first derived from the mixture viscosity using a constant Schmidt number of $Sc = 0.5$. The mole fraction based species diffusion coefficient is then defined as

$$D_i = \frac{\frac{M_i}{M}(1 - W_i)D}{1 - X_i}, \tag{8}$$

where the molecular weight of the species is given as

$$M = \left[\sum_{j=1}^{N_s} \frac{W_j}{M_j}\right]^{-1}. \tag{9}$$

Here, W and X respectively stand for the mass and mole fractions of the species; the indices i and j denote a species within a total of N_s species. Zero net mass diffusion is then ensured using the Ramshaw correction [20]. The mixing rule used in this transport model provides more reliable results when used with species of similar molecular weights. As such, it is expected to provide more accurate results for simulations with Nitrogen coolant when compared with those with Helium coolant. The physical models in TINA (original code) were not modified to match the experimental data for this work.

The mole fraction of the coolant gas (Nitrogen or Helium), X_c, in the flow field was extracted from the simulation results. A non-dimensional coolant concentration is defined as follows:

$$C(x, y) = \frac{X_c(x, y) - X_{c,e}}{1 - X_{c,e}}. \tag{10}$$

A concentration of $C = 1$ would be possible at locations where the coolant gas's mole fraction is exactly at unity, i.e. $X_c = 1$.

In order to remain consistent with the experimental concentration effectiveness, simulations with air at corresponding blowing ratios were performed and the concentration effectiveness was calculated as

$$\eta_c = 1 - \frac{X_{\text{coolant gas},w}\, p_{O_2,\text{ coolant gas},w}}{X_{\text{air},w}\, p_{O_2,\text{ air},w}}. \tag{11}$$

III. Results and Discussion

A. Coolant Concentration Distribution and Concentration Effectiveness

The coolant concentration profiles for all cases are plotted in Fig. 3 as a function of the normalised wall-normal direction. The wall-normal axis is normalised by the corresponding boundary-layer thickness, $\delta = y(0.99u_e)$, for each case (δ values are shown in Fig. 4). On the injector at $x = 165$ mm, $x = 180$ mm, $x = 198$ mm, $x = 200$ mm (blue), the concentration curves monotonically increase towards the wall. All cases apart form Case 4 feature a negative concentration gradient at the wall, i.e. $\left.\frac{\partial C}{\partial y}\right|_w < 0$. The concentration at the wall, C_w, is not at unity for these cases. The value of C_w at the injector increases with rising blowing ratio. In Case 4 (Fig. 3d), the concentration at the wall reaches $C_w = 1$ and the wall concentration gradient approaches $\left.\frac{\partial C}{\partial y}\right|_w = 0$ since the higher blowing ratio forms a discrete layer of coolant gas.

Downstream of the injector (red), the concentration curves remain monotonic but have a zero concentration gradient at the wall, i.e. $\left.\frac{\partial C}{\partial y}\right|_w = 0$, due to the impermeable wall. At larger values of x, the concentration drops in all cases (red) as the coolant mixes through diffusion with the external boundary-layer gas (consistent with the results in Ref. [10]). The curves become shallower with rising x and the peak of the curves – the wall concentration, C_w – decreases. At the

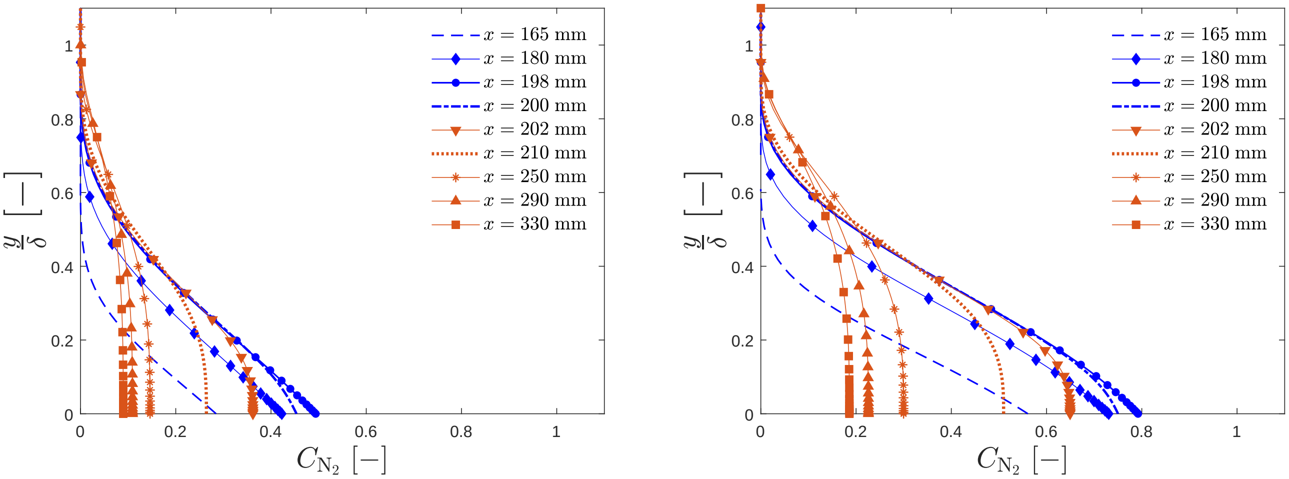

(a) Case 1, F_{N_2} = 0.0406%

(b) Case 2, F_{N_2} = 0.0818%

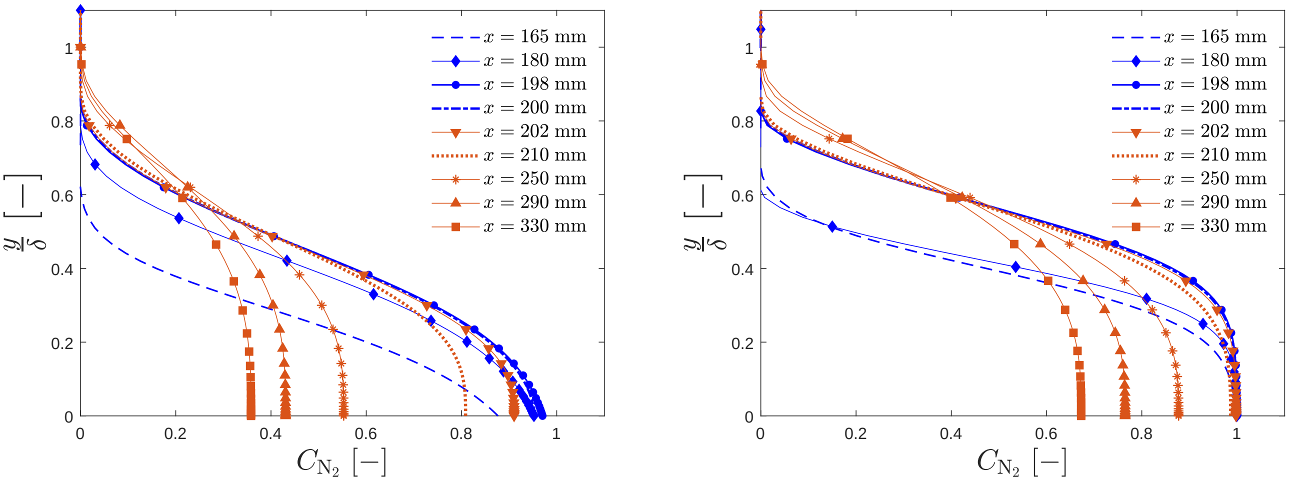

(c) Case 3, F_{N_2} = 0.153%

(d) Case 4, F_{N_2} = 0.295%

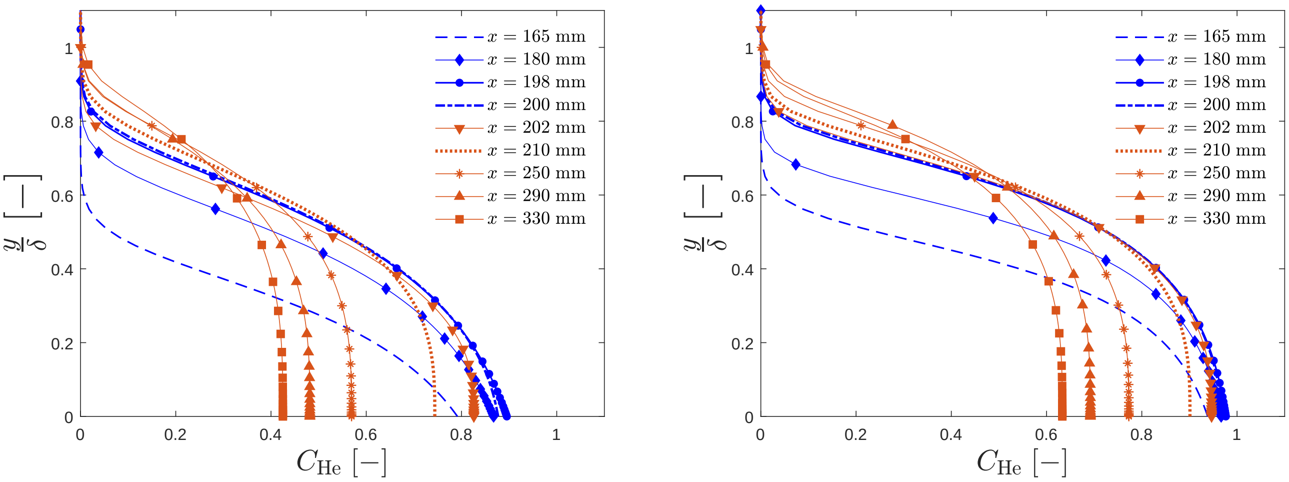

(e) Case 5, F_{He} = 0.0416%

(f) Case 6, F_{He} = 0.08%

Fig. 3 Coolant concentration profiles from numerical simulation (TINA).

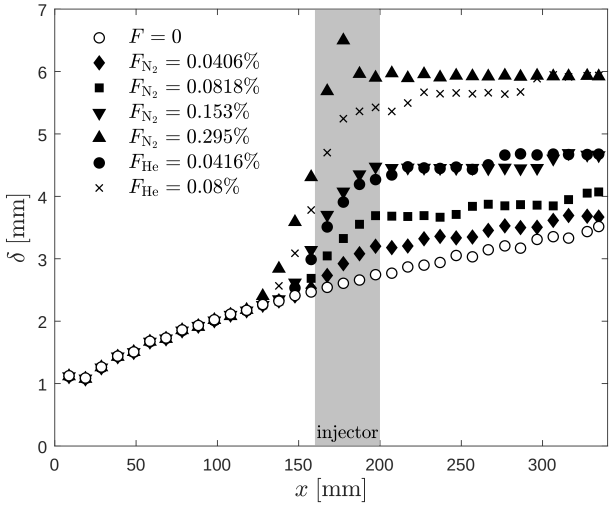

Fig. 4 Boundary-layer thickness, δ, versus stream-wise direction, x.

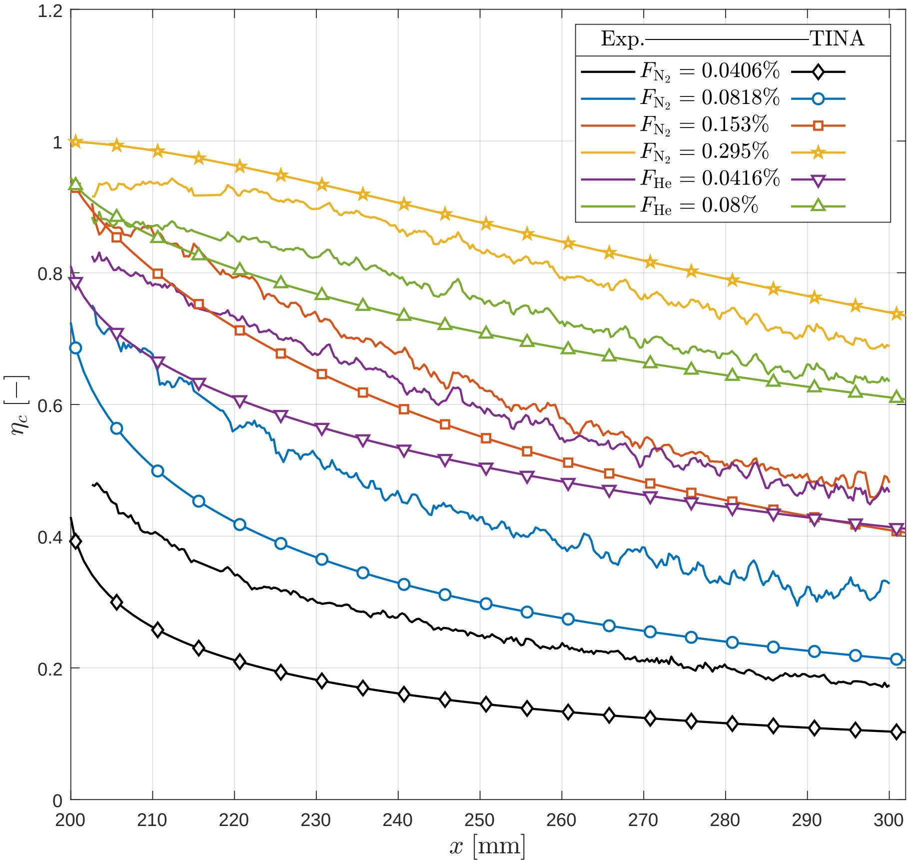

Fig. 5 Concentration effectiveness, η_c, versus stream-wise direction, x.

end of the injector ($x = 200$ mm), C_w is lower than the value of C_w at $x = 198$ mm for the lower blowing ratio cases. i.e. Cases 1, 2, and 5, due to the mixing with the external gas. The concentration gradient at the wall also becomes shallower at $x = 200$ mm compared to $x = 198$ mm as the permeable boundary condition changes to an impermeable one.

The difference between Nitrogen and Helium injection at the same blowing ratio can be observed by comparing Figs. 3a and 3b to Figs. 3e and 3f, respectively. For a given F, Helium injection results in a higher coolant coverage both at the injector and downstream thereof compared to a case of Nitrogen injection. This difference is due to Helium's seven times higher volumetric flow rate than Nitrogen's at the same mass flux, and it is consistent with the experimental finding reported in Ref. [12, 21].

In Fig. 5, the concentration effectiveness, η_c, obtained from both simulations and experiments (span-wise averaged, close to the centreline), is illustrated as a function of the stream-wise direction, x, for all cases. At the higher blowing ratio cases for each gas, i.e. Cases 3, 4, and 6, the simulation results match the experimental results within $\Delta\eta_c = \pm 0.1$. For the lower blowing ratio cases, the results differ by up to $\Delta\eta_c = \pm 0.2$. The reason for this large deviation can be attributed to the initial value of η_c immediately downstream of the injector ($x = 200$ mm). This observation indicated that the mixing process on the injector is not fully captured with the current simulation at the lower blowing ratios. The mixing on the injector is a function of the type of porous material used. It is not only dependent on the pore size and structure, but could also be influenced by the physical and aerodynamic roughness of the porous injector, especially at lower blowing ratios where only a thin layer of coolant gas is formed. As F is increased, the mixing on the injector is captured more successfully, which is evident from the initial concentration effectiveness in Fig. 5. In all cases, however, a remarkable match between the simulation results and experimental results is seen for the slope of the η_c curves, which demonstrates that the mixing rate as a function of x downstream of the injector is fully captured by the current simulations based on an advection-diffusion model. However, this is strictly limited to laminar flows at low blowing ratios, as was the case in the experiments. Injection of a gas into the boundary-layer could promote the onset of boundary-layer transition [22], and the intrinsic properties of the injected gas can affect this behaviour as demonstrated by Jewell et al. [23].

B. Thermal Effectiveness

The thermal effectiveness, η_{th}, is plotted versus the correlation factor (Eq. (5)), ξ, in Fig. 6. The values of η_{th} at $\xi < 1$ are set to unity if they are great than 1 (see Section III.C for explanation). A successful collapse of the simulation data is achieved for cases with Nitrogen injection. Similar to the observation made by Keller et al. [7], a perfect collapse of the data was not possible for the Helium cases. However, an exponent of 0.75 [12] yielded a better collapse than 0.33 [7].

For the Nitrogen cases, it can be observed that the simulation results for the higher blowing cases, i.e. Case 3 and Case 4, are close to the experimental data and the correlation proposed by Ifti et al. in Ref. [12]. Curves for the

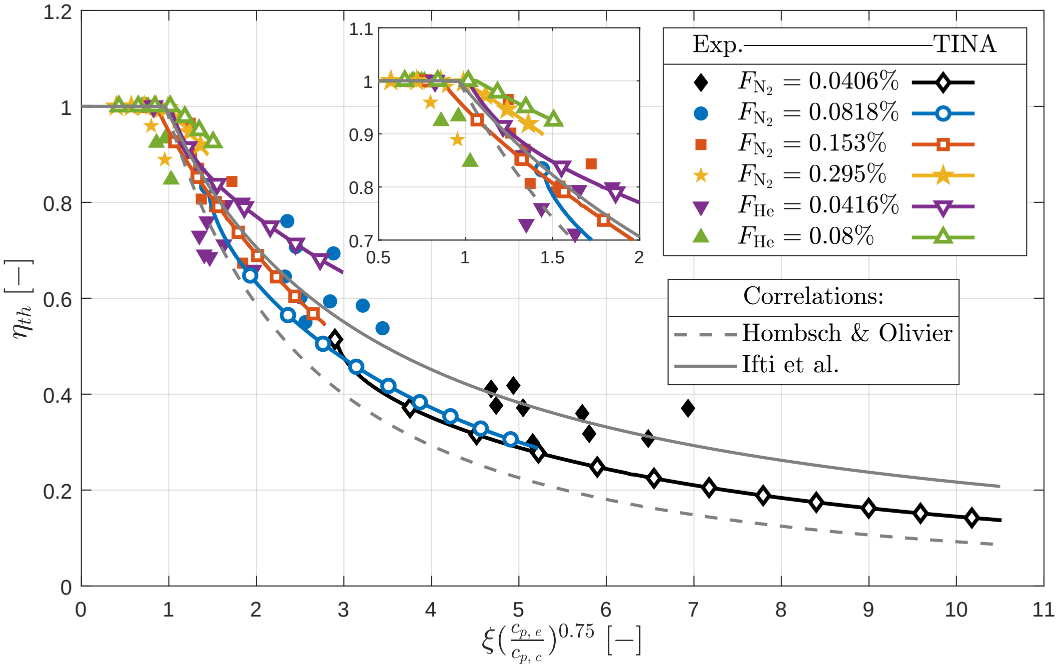

Fig. 6 Thermal effectiveness, η_{th}, versus correlation factor, ξ. Correlations from Refs. [6, 12]

smaller blowing ratio cases, on the other hand, are lower than the experimental data and the correlation curve (Ifti et al.), i.e. cooling is under-predicted by TINA. This is not surprising because the concentration effectiveness obtained from simulated data for these cases (Case 1 and Case 2) is lower than those measured in the experiments as shown in Fig. 5 and discussed in the previous section. Overall, the thermal effectiveness, η_{th}, yielded by the current simulations is within $\Delta\eta_{th} = \pm 0.1$ of the correlations for laminar flows (Hombsch & Olivier [6] and Ifti et al. [12]).

C. Boundary-Layer Profiles

As mentioned in Section III.B, the thermal effectiveness can be $\eta_{th} > 1$ at $\xi < 1$. This is because Eq.(4) is only valid for low blowing ratios and farther downstream of the injector. At higher blowing ratios and in close proximity to the injector, ξ is below 1. Theoretically, η_{th} in this region is defined as 1, but the actual value can be greater than unity due to a different flow field close to the injector at high blowing ratios. In order to gain an insight into what happens in this region, boundary-layer profiles are examined in this Section.

The normalised stream-wise velocity profiles, u/u_e, and temperature profiles, T/T_e, obtained from the simulations are illustrated in Fig. 7 and Fig. 8, respectively, for all blowing cases. The wall-normal axis is normalised by the boundary-layer thickness, δ. A close-up view of the wall-near region is placed as an inset in every sub-figure. Profiles are picked at x = 100 mm (upstream of the injector, black), x = 180 mm (middle of the injector, blue), x = 200 mm (end of the injector, blue), x = 210 mm (10 mm downstream of the injector, red), and x = 330 mm (130 mm downstream of the injector, red).

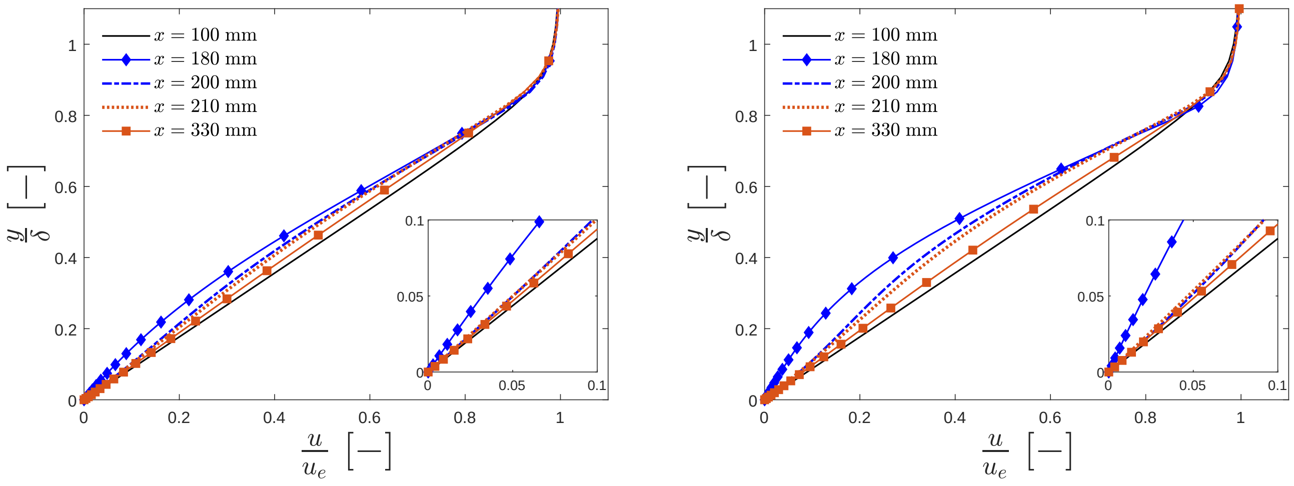

(a) Case 1, $F_{\mathrm{N_2}}$ = 0.0406%

(b) Case 2, $F_{\mathrm{N_2}}$ = 0.0818%

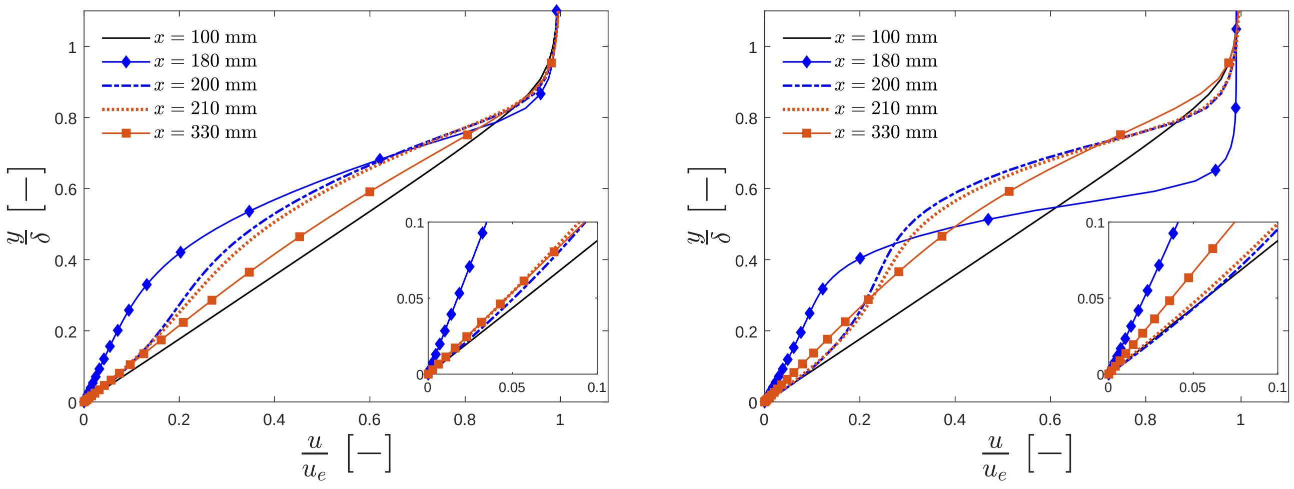

(c) Case 3, $F_{\mathrm{N_2}}$ = 0.153%

(d) Case 4, $F_{\mathrm{N_2}}$ = 0.295%

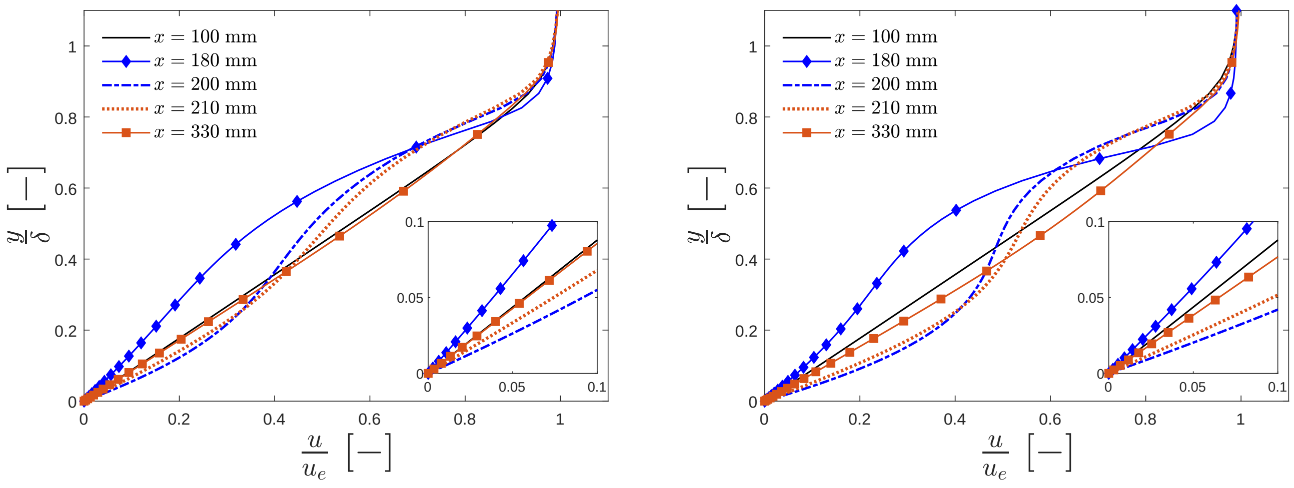

(e) Case 5, F_{He} = 0.0416%

(f) Case 6, F_{He} = 0.08%

Fig. 7 Normalised stream-wise velocity profiles from numerical simulations (TINA).

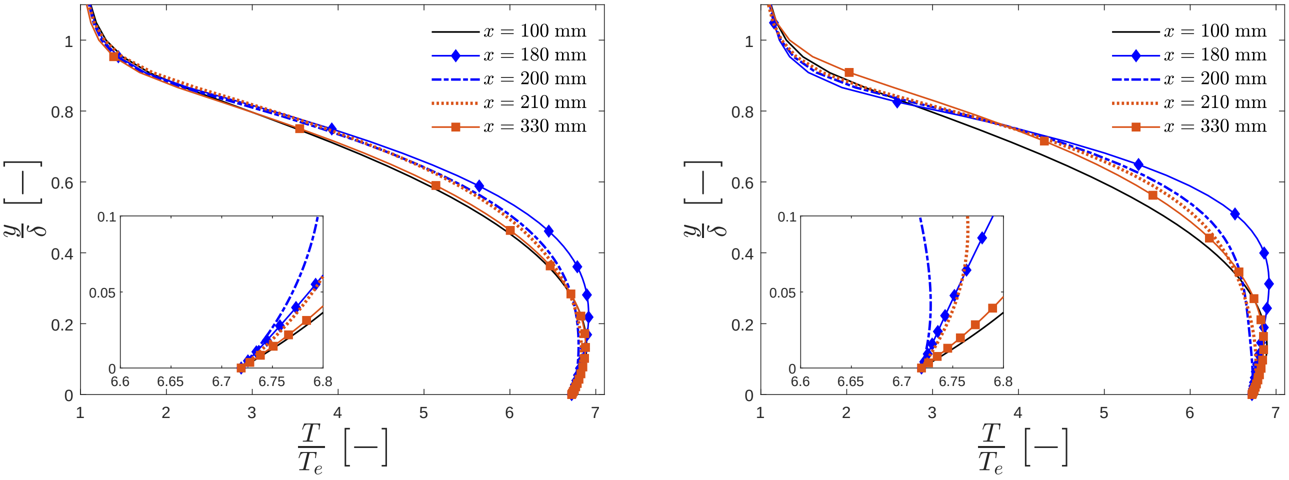

(a) Case 1, F_{N_2} = 0.0406% (b) Case 2, F_{N_2} = 0.0818%

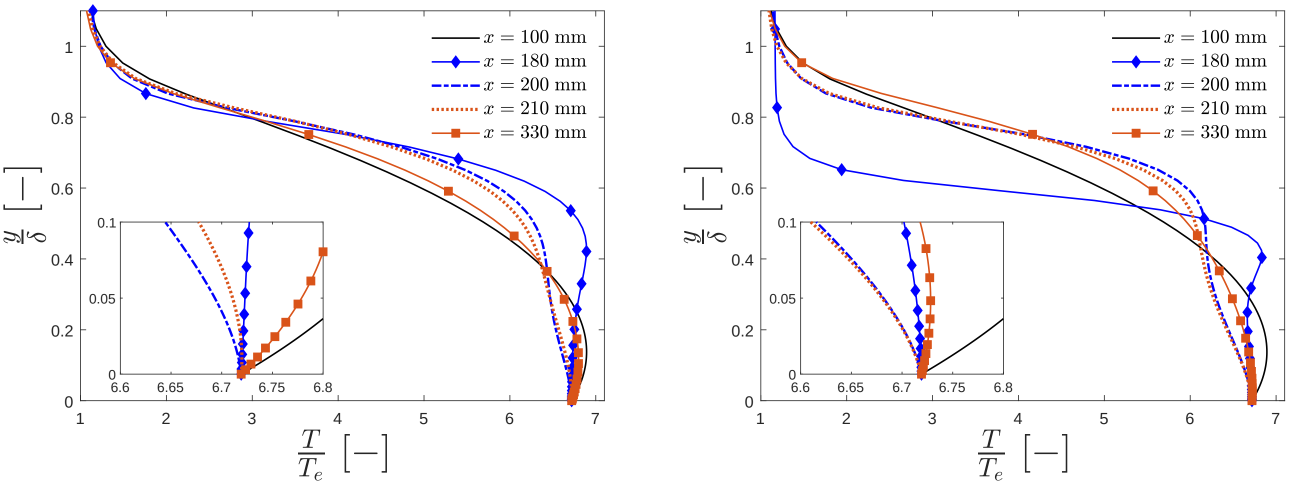

(c) Case 3, F_{N_2} = 0.153% (d) Case 4, F_{N_2} = 0.295%

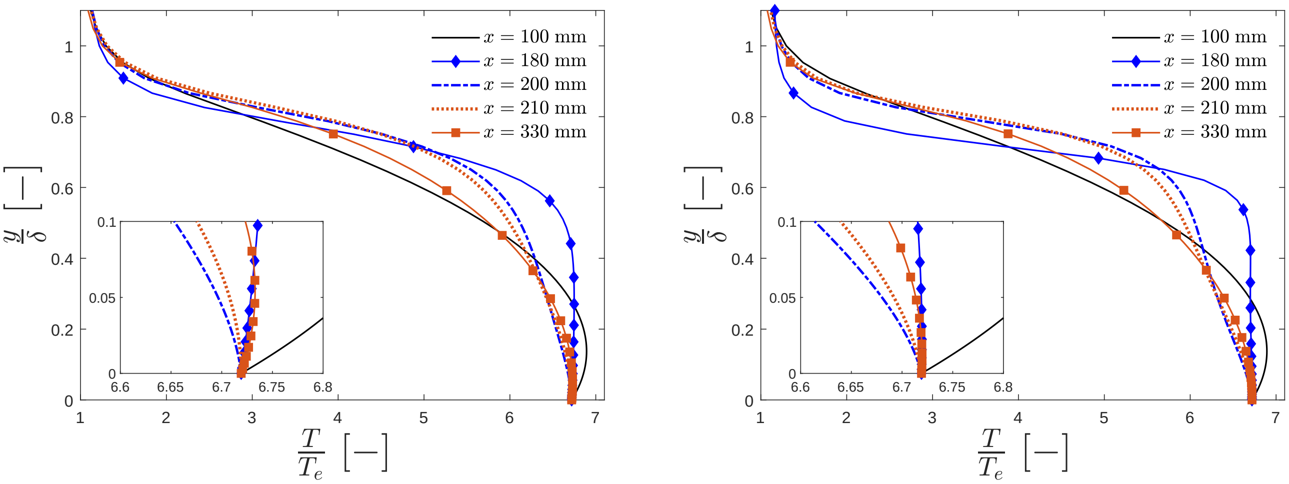

(e) Case 5, F_{He} = 0.0416% (f) Case 6, F_{He} = 0.08%

Fig. 8 Normalised temperature profiles from numerical simulations (TINA).

In Fig. 7, it can be seen that the velocity profile (black) represents a Blasius profile [24] for laminar boundary-layers at zero pressure gradient upstream of the injector. On the injector, the profiles (blue) inflect due to the low stream-wise velocity from blowing (injected coolant gas only has a wall-normal velocity at the wall). As expected, the higher blowing ratio cases cause a stronger inflection. However, no separation of the boundary-layer is observed for the simulated cases.

In the Nitrogen cases (Fig. 7a-d), the velocity profiles downstream of the injector become fuller as the coolant gas is accelerated in the stream-wise direction by shear stress from the external boundary-layer flow. At larger x values, the profiles approaches the Blasius profile (trend seen in profiles at $x = 210$ mm and $x = 330$ mm). In contrast, the velocity profiles immediately downstream of the injector become fuller than the Blasius profile in the Helium cases (see profile at $x = 210$ mm in Figs. 7e and 7f). This is due to the difference in density between Helium and Nitrogen. This behaviour is also visible for profiles at the end of the injector, i.e. at $x = 200$ mm.

The temperature profiles upstream of the injector (black) exhibit a typical non-monotonic trend with a positive gradient at the wall, i.e. $\left.\frac{\partial T}{\partial y}\right|_w > 0$, resulting in heating of the wall. This non-monotonic trend is present on the injector (blue) for Cases 1, 2, and 5. At higher blowing ratios, however, the trend changes as the gradient at the wall approaches $\left.\frac{\partial T}{\partial y}\right|_w = 0$ (see inset, Fig. 8c, 8d, and 8f). As the coolant is injected at the wall temperature, T_w, the injection builds up a layer of gas at wall temperature.

At $x = 200$ mm (end of the injector) and $x = 210$ mm (10 mm downstream of the injector), the profiles drop below the wall temperature in Cases 3 to 6 (see inset, Fig. 8c-f). In Cases 4 (Fig. 8d) and 6 (Fig. 8f), the temperature drops so much so that the gradient at the wall becomes negative, i.e. $\left.\frac{\partial T}{\partial y}\right|_w < 0$, resulting in a negative heat flux. This phenomenon is captured in heat flux data obtained from the current simulations as well as the experiments as presented in Fig. 9. This phenomenon is also present close to the injector in the work by Keller et al. [7], Heufer & Olivier [5, 25], and Hombsch & Olivier [6], where the coolant temperature was close to the wall temperature. These authors reported a thermal effectiveness greater than 1, i.e. $\eta_{th} > 1$ very close to the injector and at $\xi < 1$, which indicates a negative heat flux occurred at those locations. ξ reduces for higher F values and lower x values, and therefore the phenomenon of negative heat flux appears close to the injector at higher blowing ratios as seen in Case 4 and Case 6. This phenomenon is discussed in the following paragraph.

When the coolant is injected at a higher blowing ratio, it forms an almost complete layer of coolant gas on the porous injector, and immediately downstream of it. This gas is initially close to zero stream-wise velocity when it is injected (see Figs. 7d and 7f). The temperature of the injected gas is approximately the wall temperature T_w (see Figs. 8d and 8f). On the porous injector and immediately downstream of it, this creates a boundary layer profile of almost stagnant gas at wall temperature, i.e. a constant profile of T_w from the wall to the coolant layer height.

Upon getting into contact with the external cross flow the coolant gas layer is accelerated due to the shear stress of the external flow (see profile at $x = 210$ mm in Figs. 7d and 7f). This leads to the coolant gas establishing a velocity profile which leads to dissipation of thermal energy (the term $\mu(\partial u/\partial y)^2$ in energy equation). Classically this effect is expressed as a recovery factor $T_r = rT_0$, i.e. the driving temperature of the heat transfer is lower than the total temperature T_0. In this case, the total temperature of the coolant layer is close to the the wall temperature, as the injected gas started at near zero stream-wise velocity at T_w. Therefore, the driving temperature of the wall heat transfer can only be lower than the wall temperature (as shown in Figs. 8d and 8f) and a negative heat flux is experienced. This effect only applies if the film is almost entirely comprised of coolant gas, i.e. η_c of close to 1. Fig. 9 shows that only cases with high η_c promote a Stanton numbers below zero (Cases 4 and 6). Although there is a discrepancy between the results obtained from TINA and the experiments, the trend of negative heat flux is captured in both. In cases where η_c is significantly below 1, hot external gas has already mixed with the coolant layer which drives the effective recovery temperature up and therefore increases heat transfer. In Fig. 10, the temperature profiles at x = 210 mm and x = 330 mm for all cases are plotted. It can be observed that close to the injector (see Fig. 10a), the temperature gradient change from positive to negative as the blowing ratio is increased. The temperature gradient becomes negative for Cases 4 and 6, which results in a negative heat flux (see Fig. 9). Farther downstream (see Fig. 10b), no negative temperature gradient exists regardless of the blowing ratio.

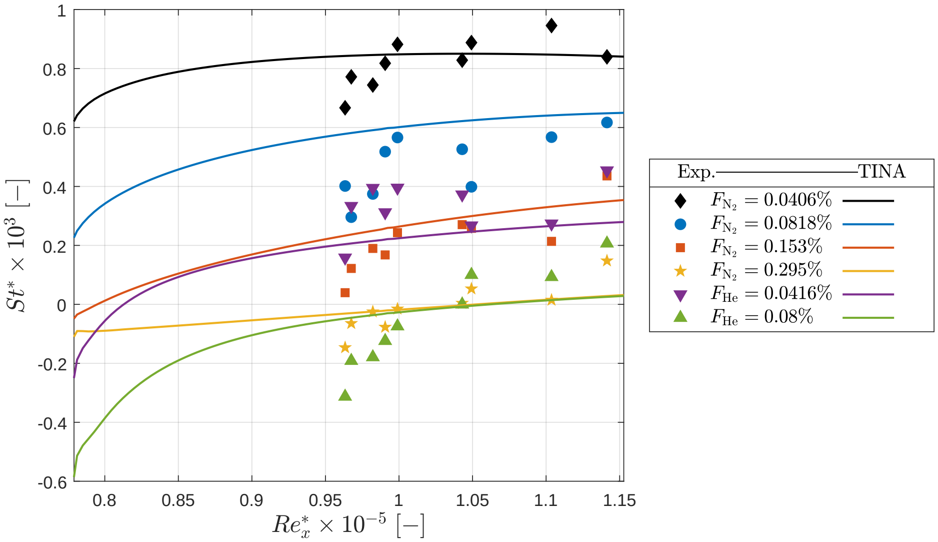

Fig. 9 Stanton number, St^*, versus Reynolds number based on stream-wise direction starting from the leading edge, Re_x^*. The plot shows values starting from immediately downstream of the injector. St^* and Re_x^* are evaluated at Eckert's reference temperature [13].

This effect is stronger for Helium because it is a lighter gas. It is accelerated more than the heavier Nitrogen and an established velocity profile is reached earlier downstream of the injector (Fig. 7f, x = 210 mm). This leads to a higher shear stress in the boundary layer which promotes larger energy dissipation. Therefore, the driving temperature in the Helium cases is lower and the negative heat flux is more pronounced (Fig. 9). This trend is even stronger at the end of the injector, i.e. at x = 200 mm.

Counteracting effects are mixing, i.e. diffusive mass transfer of hot gas into the coolant layer for laminar flows, and

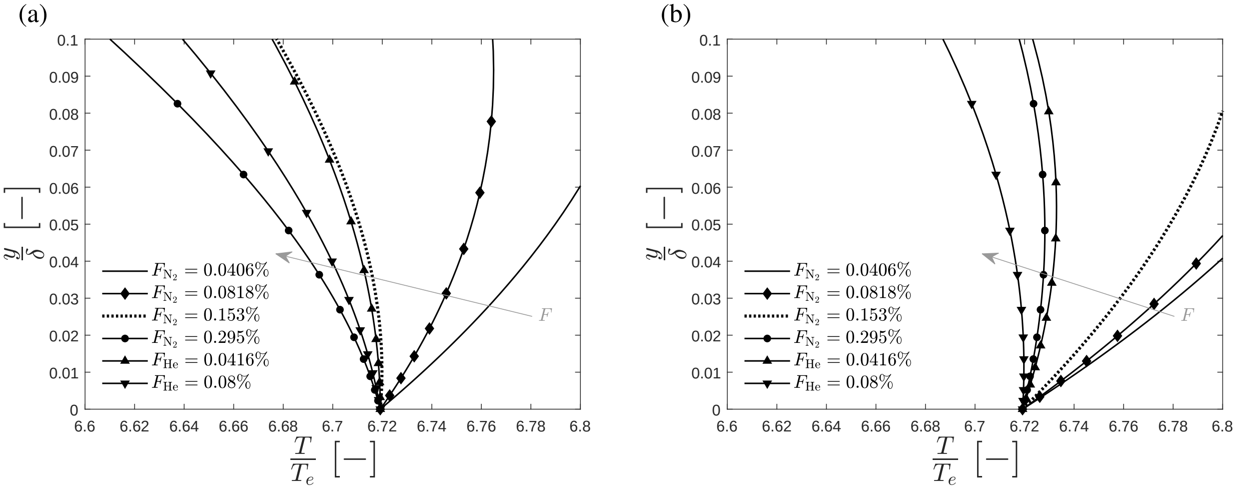

Fig. 10 Normalised temperature profiles at (a) x = 210 mm **and (b)** x = 330 mm **for all cases (TINA).**

heat conduction from the outside flow. These two effects thus diminish the negative heat flux by effectively increasing the driving temperature of the surface heat transfer. For high η_c, the dissipative effect dominates, whilst mixing and heat conduction dominate for cases with low η_c (visible in Fig. 9).

IV. Conclusion

In this work, two-dimensional simulations of transpiration cooling in a laminar, hypersonic boundary-layer were performed employing the Thermochemical Implicit Non-Equilibrium Algorithm (TINA) – a Navier-Stokes solver developed by Fluid Gravity Engineering Ltd. Coolant concentration and heat flux results are compared to data obtained from laminar transpiration cooling experiments conducted in the Oxford High Density Tunnel (HDT) employing a flat-plate geometry at Mach 7. Simulations for six different blowing ratios are performed using Nitrogen and Helium as the coolant gas. The concentration effectiveness matches the experimental data within ±0.1 for higher blowing ratios and ±0.2 for lower blowing ratios. The simulation results successfully predict the mixing rate at the wall as a function of the stream-wise direction for all blowing ratios. This shows that the simulations are not as successful in predicting the mixing on the injector at low blowing ratios as they are downstream of the injector. The simulations further demonstrate that the mixing process at the wall can be predicted by an advection-diffusion model. A collapse of thermal effectiveness calculated from simulation data is achieved using a laminar film cooling correlation factor, which lies within ±0.1 of the correlations for laminar flows in the literature. Wall-normal profiles of coolant concentration, stream-wise velocity, and temperature are examined upstream, at the middle, and downstream of the injector. It is shown that, when the concentration effectiveness is close to 1 at the injector, the temperature gradient becomes negative at locations immediately downstream of the injector, resulting in a negative heat flux. This phenomenon of negative heat flux is captured both in the experiments and the current simulations. It is evident from the velocity profiles that the coolant is accelerated in the stream-wise direction downstream, which promotes dissipation of energy. This results in a reduction in the temperature of the coolant that is injected at the wall temperature and thereby induces a negative temperature gradient that leads to negative heat flux in close proximity to the injector.

Acknowledgements

The funding for this research by the EPSRC grant 'Transpiration Cooling Systems for Jet Engine Turbines and Hypersonic Flight' (reference: EP/P000878/1) is gratefully acknowledged. The authors would like to thank Craig Parsons of Oxford Thermofluids Institute for his IT support in this work.

References

[1] van Driest, E. R., "The Problem of Aerodynamic Heating," *Aeronautical Engineering Review*, Vol. 15, No. 10, 1956, pp. 26–41.

[2] Goldstein, R. J., "Film Cooling," *Advances in Heat Transfer*, Vol. 7, 1971, pp. 321–379. https://doi.org/10.1016/S0065-2717(08)70020-0.

[3] Fujiwara, K., Sriram, R., Kontis, K., and Ideta, T., "Review on Film Cooling in High-Speed Flows," *31st International Symposium on Shock Waves 2*, Springer, Cham, 2017, pp. 939–946. https://doi.org/10.1007/978-3-319-91017-8_118.

[4] Richards, B. E., and Stollery, J. L., "Laminar Film Cooling Experiments in Hypersonic Flow," *Journal of Aircraft*, 1979. https://doi.org/10.2514/3.58502.

[5] Heufer, K. A., and Olivier, H., "Experimental and Numerical Study of Cooling Gas Injection in Laminar Supersonic Flow," *AIAA Journal*, 2008. https://doi.org/10.2514/1.34218.

[6] Hombsch, M., and Olivier, H., "Film Cooling in Laminar and Turbulent Supersonic Flows," *Journal of Spacecraft and Rockets*, 2013. https://doi.org/10.2514/1.A32346.

[7] Keller, M. A., Kloker, M. J., and Olivier, H., "Influence of Cooling-Gas Properties on Film-Cooling Effectiveness in Supersonic Flow," *Journal of Spacecraft and Rockets*, 2015. https://doi.org/10.2514/1.A33203.

[8] Brune, A., Hosder, S., Gulli, S., and Maddalena, L., "Variable Transpiration Cooling Effectiveness in Laminar and Turbulent Flows for Hypersonic Vehicles," *AIAA Journal*, 2014. https://doi.org/10.2514/1.J053053.

[9] Gülhan, A., and Braun, S., "An experimental study on the efficiency of transpiration cooling in laminar and turbulent hypersonic flows," *Experiments in Fluids*, Vol. 50, No. 3, 2010, pp. 509–525. https://doi.org/10.1007/s00348-010-0945-6.

[10] Jewell, J. S., "Boundary-Layer Transition on a Slender Cone in Hypervelocity Flow with Real Gas Effects," Ph.D. thesis, 2014. https://doi.org/10.7907/Z9H9935V.

[11] Hermann, T., McGilvray, M., and Naved, I., "Performance of Transpiration-Cooled Heat Shields for Reentry Vehicles," *AIAA Journal*, 2019. https://doi.org/10.2514/1.J058515.

[12] Ifti, H. S., Hermann, T., Ewenz Rocher, M., Doherty, L., Hambidge, C., McGilvray, M., and Vandeperre, L. J., "Laminar Transpiration Cooling Experiments in Hypersonic Flow," *Experiments in Fluids*, 2022. https://doi.org/10.1007/s00348-022-03446-1.

[13] Eckert, E. R. G., "Engineering Relations for Heat Transfer and Friction in High-Velocity Laminar and Turbulent Boundary-Layer Flow over Surfaces with Constant Pressure and Temperature," *Transactions of the American Society of Mechanical Engineers*, Vol. 78, No. 6, 1956, p. 1273.

[14] Netterfield, M. P., "Hypersonic Aerothermodynamic Computations Using a Point - Implicit TVD Method," *First European Symposium on Aerothermodynamics for Space Vehicles, ESTEC*, 1991.

[15] Netterfield, M. P., "Validation of a Navier Stokes Code for Thermochemical Non Equilibrium Flows," *AIAA Twenty-Seventh Thermophysics Conference*, 1992.

[16] Blottner, F. G., Johnson, M., and Ellis, M., "Chemically Reacting Viscous Flow Program for Multi-Component Gas Mixtures." Tech. Rep. SC-RR-70-754, Jan. 1971. https://doi.org/10.2172/4658539.

[17] Eucken, A., "Über das Wärmeleitvermögen,die spezifische Wärme und die innere Reibung der Gase," *Zeitschrift für Physik*, Vol. 14, 1913, pp. 324–332.

[18] Wilke, C. R., "A Viscosity Equation for Gas Mixtures," *The Journal of Chemical Physics*, Vol. 18, No. 4, 2004, p. 517. https://doi.org/10.1063/1.1747673.

[19] Lee, J.-H., "Basic Governing Equations for the Flight Regimes of Aeroassisted Orbital Transfer Vehicles," *19th Thermophysics Conference*, Snowmass, CO, USA, 1984. https://doi.org/10.2514/6.1984-1729.

[20] Ramshaw, J. D., "Self-Consistent Effective Binary Diffusion in Multicomponent Gas Mixtures," *Journal of Non-Equilibrium Thermodynamics*, Vol. 15, 1990, pp. 295–300. https://doi.org/10.1515/jnet.1990.15.3.295.

[21] Langener, T., Wolfersdorf, J. V., and Steelant, J., "Experimental Investigations on Transpiration Cooling for Scramjet Applications Using Different Coolants," *AIAA Journal*, Vol. 49, No. 7, 2011, pp. 1409–1419. https://doi.org/10.2514/1.J050698.

[22] Schneider, S. P., "Hypersonic Boundary-Layer Transition with Ablation and Blowing," *Journal of Spacecraft and Rockets*, Vol. 47, No. 2, 2012, pp. 225–237. https://doi.org/10.2514/1.43926.

[23] Jewell, J. S., Leyva, I. A., Parziale, N. J., and Shepherd, J. E., "Effect of Gas Injection on Transition in Hypervelocity Boundary Layers," *28th International Symposium on Shock Waves*, Springer, Berlin, Heidelberg, 2012, pp. 735–740. https://doi.org/10.1007/978-3-642-25688-2_111.

[24] Blasius, H., "Grenzschichten in Flüssigkeiten mit kleiner Reibung," *Zeitschrift für angewandte Mathematik und Physik*, Vol. 56, 1908, pp. 1–37.

[25] Heufer, K. A., and Olivier, H., “Experimental Study of Active Cooling in 8 Laminar Hypersonic Flows,” *RESPACE – Key Technologies for Reusable Space Systems*, Springer, Berlin, Heidelberg, 2008, pp. 132–150. https://doi.org/10.1007/978-3-540-77819-6_8.